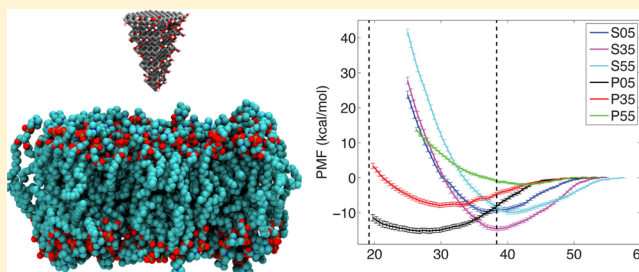# Free Energy Calculation of Nanodiamond-Membrane Association—The Effect of Shape and Surface Functionalization

Zhenpeng Ge,[†] Quan Li,[†,‡] and Yi Wang*,[†]

[†]Department of Physics, Chinese University of Hong Kong, Shatin, Hong Kong
[‡]Chinese University of Hong Kong Shenzhen Research Institute, Shenzhen, China

S *Supporting Information*

ABSTRACT: Nanodiamonds (NDs) are nanoscale diamond particles with broad applications in biosensing, drug delivery, and long-term tracking. Their interactions with a membrane dictate both the endocytosis process and subsequent intracellular fate of the nanoparticles. However, details of ND-membrane association and the energetics of this process remain largely unknown. In this work, we use all-atom molecular dynamics (MD) simulations to determine the free energy profile and molecular details of ND-membrane association, with a focus on the impact of shape and surface

functionalization. Through altogether 6.5 μs umbrella sampling on six atomistic ND models of different shapes (spherical or pyramidal) and surface functionalization (5%, 35%, and 55%), we show that nanodiamonds associate favorably with the membrane, which is largely driven by ND−lipid interactions. During its membrane association, the shape of a nanodiamond plays a key role in determining the location of the free energy minimum, while its surface functionalization modulates the depth of the minimum. Of the six models studied here, all spherical NDs adhere to the bilayer surface, whereas pyramidal NDs, with the exception of the most functionalized P55, anchor inside the membrane. Shape also dominates the height of the free energy barrier: the sharp pyramidal NDs have much lower barriers against penetrating a POPC bilayer than spherical ones. Our all-atom ND models and their bilayer association strength determined here can be combined with future coarse-grained or continuum models to further explore ND−membrane interactions on larger length scales.

■ INTRODUCTION

Nanoparticles have broad applications in biosensing, cellular imaging, and intracellular delivery of various cargoes, such as DNAs, siRNAs, and drug molecules.[1−3] A major route of their cellular entrance is endocytosis, during which they are engulfed by the cell and reside in lipid vesicles named endosomes.[4,5] Apart from experimental studies,[6−8] the endocytosis of nanoparticles has been the subject of extensive computational work.[9−12] For instance, results from continuum modeling[11,12] indicate that this process can be understood as a competition between elastic deformation energy and nanoparticle−membrane attraction— while the bending rigidity and surface tension of a membrane oppose the uptake of the particle, the attraction between the two parties favors this process. Interactions with a membrane not only affect endocytosis, but also play a key role in determining the intracellular fate of nanoparticles. Once they are inside a cell, the next stop of nanoparticles is determined by whether they can penetrate the endosomal membrane: if so, they enter the cytoplasm, often an ideal location for biosensing and cargo delivery; otherwise, they are subjected to changes in the chemical/biological environment as an endosome matures and can be eventually excreted through exocytosis, the reverse process of endocytosis.

In recent years, nanoparticle−membrane interactions have been increasingly studied with molecular dynamics (MD)
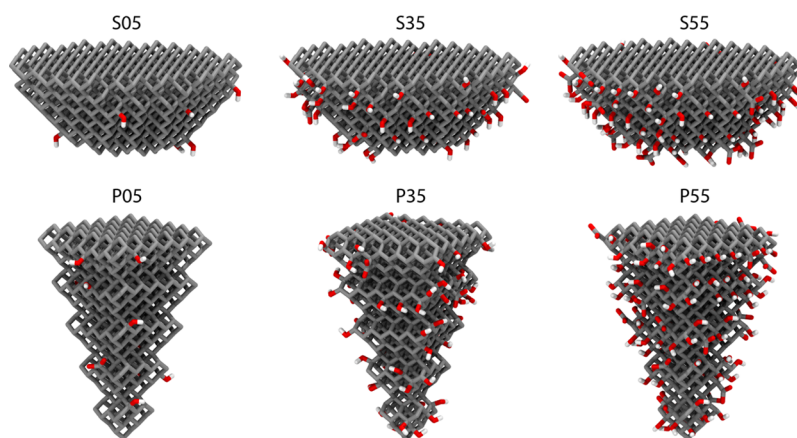
simulations.[13−18] The MARTINI coarse-grained (CG) force field, for example, is widely used in such studies (see ref 19 and references therein). A CG model with further reduced granularity has also been developed, where a phospholipid is represented by three beads[20] and certain headgroup beads can be assigned an attractive interaction with the nanoparticle. Using this model, Vácha et al. studied receptor-mediated endocytosis[21] and pH-induced release of endocytosed nanoparticles.[22] Additionally, dissipative particle dynamics (DPD) simulations have been performed to examine the translocation of nanoparticles across a membrane.[23,24] Compared with CG MD or DPD simulations, all-atom MD has higher spatial resolution, although this advantage is normally achieved at the cost of system size and simulation length. Therefore, only a limited number of all-atom simulations have been performed to study the interactions of nanoparticles with a membrane.[25−29]

In this work, we focus on nanodiamonds (NDs), which are nanoscale diamond particles with wide applications in drug delivery, ultrasensitive biosensing, as well as long-term

Figure 1. Nanodiamonds studied in this work. Except for their top surfaces, the pyramidal (P) and spherical (S) NDs are functionalized at 5%, 35%, and 55% by two functional groups (−OH or −COO⁻). Structure files and force field parameters of all NDs are provided in the Supporting Information.

tracking.[30−32] Our goal is to examine the energetics and molecular details of ND−membrane association, with a focus on the impact of shape and surface hydrophilicity. To this end, we constructed six atomistic ND models with different shapes (spherical or pyramidal) or surface functionalization (5%, 35%, or 55% of surface atoms). As NDs are negatively charged at pH ≈ 7 due to surface oxidation, two types of functional groups (−OH or −COO⁻) were modeled using the CHARMM general force field (cGenFF).[33] Thus, surface functionalization determines the hydrophilicity of our ND models: the more functionalized a ND is, the more hydrophilic its surface becomes. Using these models, we performed altogether 6.5 μs umbrella sampling to determine the potential of mean force (PMF) as NDs approach a POPC bilayer. Results of our calculation indicate that the negatively charged nanodiamonds associate favorably with the membrane, during which their shape plays a key role in determining the location of the free energy minima, while their surface functionalization modulates the depth of the minima. Notably, NDs of different shapes tend to have different interaction modes with the bilayer: while spherical NDs adhere to the bilayer surface, pyramidal NDs are more likely to anchor in the membrane. The latter NDs also have much lower energy barriers of penetrating the bilayer, consistent with a recent experiment[34] where only NDs with sharp corners spontaneously escape from the endosome.
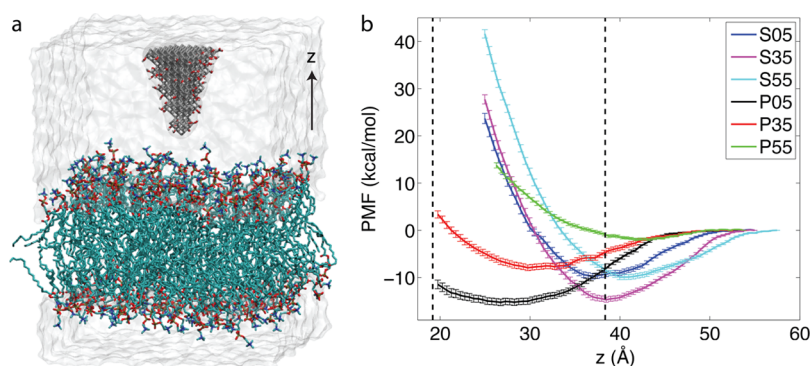
■ METHODS

Model Construction and Parametrization. Six nanodiamond models with different shapes and surface functionalization were constructed (Figure 1). We began by replicating a diamond unit cell in space and then cut the bulk diamond into a pyramid or a spherical cap. The former has a square top surface of 15 Å by 15 Å and a height of 25 Å, while the latter is approximately a semisphere with a radius of 15 Å. For simplicity, we will refer to them as pyramidal ND and spherical ND, respectively. Such truncated ND models can be considered as representing the tip of a nanodiamond used in a recent experiment,[34] which has an average size of ∼115 nm. Excluding atoms on the top surface, the pyramidal and spherical NDs have a similar number of surface carbons (219 and 196, respectively), which are defined as carbons with less than four neighboring atoms. To mimic NDs' oxidized surface[35−37] with different hydrophilicity, we selected approximately 5%, 35%, and 55% of surface carbons at random and functionalized them with

hydroxyl (−OH) or carobxylate (−COO⁻) groups at a molar ratio of 7:1. The remaining surface carbons and carbons on the top surface are terminated by hydrogen atoms. We should note that nanodiamonds used in experiments have more complex surfaces:[32] apart from various functional groups, surface carbons may exist in both sp³ and sp² forms, although the oxidation process tends to remove the latter.[35−37] Modeling of an all-atom nanodiamond as described above faces another complexity: steric clashes must be monitored throughout the functionalization process, in order to avoid, for instance, adding COO⁻ groups to neighboring surface carbons, which may place their atoms too close to each other. Due to such steric clashes, the highest surface functionalization we could achieve with the all-atom sp³ ND model is ∼65%.

Following the construction of the above ND models, we used ParamChem[38,39] to assign atom types and atomic partial charges for the functional groups. Interior carbon atoms, i.e., carbons with four neighboring carbons, were given a zero atomic partial charge. To simplify the modeling of different ND surfaces,[40] nonpolar hydrogens were not modeled explicitly. Instead, we used a united atom model for carbons bonded to 1, 2, or 3 hydrogens. Parameters for these carbons were obtained from Hénin et al.[41] and subsequently validated by comparing the radial pair distribution function of water surrounding the united-atom ND model and an all-atom ND model with explicit hydrogens (Figure S1). Bond, angle, and dihedral parameters were taken from bulk diamond (if available) or by analogy to existing cGenFF parameters. All ND structures and force field parameters are provided in the Supporting Information.

Finally, we constructed the ND-membrane systems by combining the above ND models with a POPC bilayer. The bilayer has 85 lipids in each monolayer and was previously equilibrated in a 1-μs simulation performed on the specialized machine Anton.[42] Using the autoionize plugin of VMD,[43] the ND-membrane systems are neutralized by adding sodium and chloride ions at a concentration of 0.1 mol/L. The final systems contain ∼56 000 atoms, with a size of approximately 76 × 76 × 98 Å³. Based on the different shapes (spherical cap or pyramid) and surface functionalization of their ND models, we will refer to these systems as S05, S35, S55, P05, P35, and P55, respectively (Figure 1).

Umbrella Sampling. The ND-membrane systems constructed above are minimized for 5000 steps and equilibrated for 3 ns, in order to relax water molecules surrounding the newly

Figure 2. Side view of the simulation box (a) and the PMFs obtained from umbrella sampling (b). Water molecules are shown as a transparent surface in a. In all PMF calculation and subsequent analysis, $z = 0$ is placed at the c.o.m. of bottom-monolayer phosphorus atoms. The location of the bilayer center ($z = 19.2$ Å) and the c.o.m. of upper-monolayer phosphorus atoms ($z = 38.4$ Å) are shown as dashed lines in b.

introduced ND. Starting from the end structures of the equilibration, we performed up to 40 ns steered molecular dynamics (SMD) simulation[44−46] to pull the NDs toward the membrane at a speed of 1 Å/ns. In both SMD and subsequent umbrella sampling, we set the reaction coordinate to be the distance between the nanodiamond and the membrane projected along the z axis. Specifically, as the top lipid monolayer is significantly perturbed upon contacting the nanodiamond, we choose the center-of-mass (c.o.m.) of phosphorus atoms from the bottom lipid monolayer as the reference point. The distance between this reference point and the bottom central carbon on a ND is measured, and its projection along the z axis is used in SMD and umbrella sampling calculations. We should add that unlike pyramidal NDs, the bottom central carbon is 1.778 Å away from the bottom carbons in spherical NDs (Figure S2). Therefore, we shifted the PMFs of all spherical NDs by −1.778 Å to ensure a fair comparison with the pyramidal NDs. The same treatment is used in all analyses of spherical NDs.

The SMD simulations generated a set of starting frames in the range of $z \approx 20$ Å to $z \approx 60$ Å, which are used in the subsequent umbrella sampling calculation. For each ND system, 19 to 23 umbrella windows are used at a spacing of 1.5 Å. Once a ND reaches its free energy minimum, an additional ∼10 Å region is sampled, resulting in a left boundary of $z \approx 20$ Å for P05 and P35 and $z \approx 25$ Å for the remaining NDs. Depending on whether the free energy profiles "plateau out" in bulk water, additional windows are used for some systems. Each umbrella window is simulated for 50 ns, with a force constant of 4 kcal/mol/Å². In both SMD and umbrella sampling, the distance between the ND top and bottom central carbons, projected on the xy plane, is constrained at zero with a force constant of 100 kcal/mol/Å². This constraint, achieved through the collective variable module[47] of NAMD,[48] ensures that the nanodiamond does not "tilt" during the simulation. Therefore, the resulting PMFs represent free energy profiles with ND orientation fixed at a specific value. The impact of varying ND orientation is discussed in the following section.
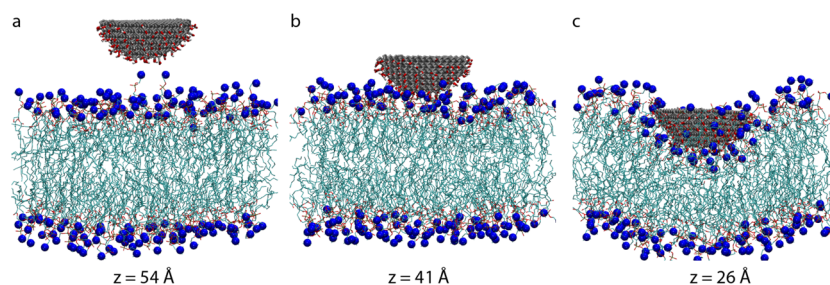
Simulation Protocols. All simulations were performed with the 2.9 release of NAMD,[48] with the cGenFF[33] force field for small molecules and the CHARMM36[49] force field for lipids. The top surface of an ND, which arises from cutting a bulk diamond, was treated with extra bonds to avoid any conformational change of this artificial surface: the distance between adjacent carbons separated by 2.51 Å was constrained with a force constant of 890 kcal/mol/Å². A time step of 2 fs was adopted in all simulations, with bonds involving hydrogen atoms

constrained using RATTLE[50] and water geometries maintained using SETTLE.[51] The multiple-time-stepping algorithm was used, with short-range forces calculated every step and long-range electrostatics calculated every two steps. The cutoff for short-range nonbonded interactions was set to 12 Å, with a switching distance of 10 Å. The CHARMM force switching was used for vdW forces, in order to be consistent with the CHARMM36 force field for lipids.[49] Assuming periodic boundary conditions, the Particle Mesh Ewald (PME) method[52] with a grid density of at least 1/Å³ was employed for computation of long-range electrostatic forces. Langevin dynamics with a damping coefficient of 1 ps^{-1} was used to keep the temperature constant at 310 K, while a Nosé−Hoover−Langevin piston[53] was used to keep the pressure constant at 1 atm. The pressure control was performed semi-isotropically: the z axis of the simulation box, which is normal to the membrane, was allowed to fluctuate independently from the x and y axes. To better illustrate the above simulation protocols, an example simulation input file is provided in the Supporting Information.
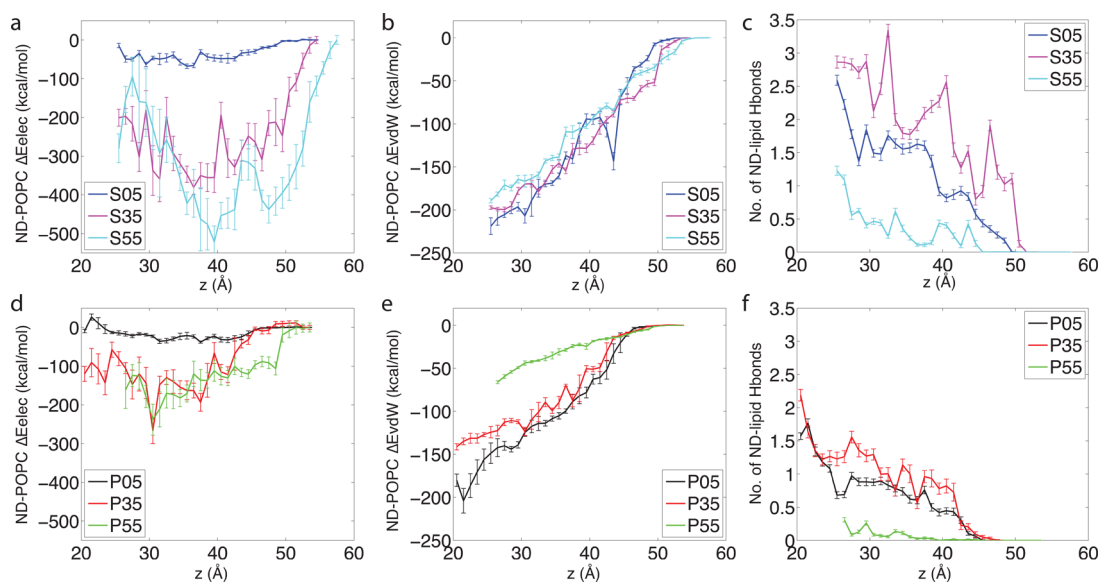
Analysis. The GROMACS tool g_wham is used to construct the PMFs, with the error estimated through 1000 rounds of bootstrapping analysis using the "trajectory" method.[54] The first 5 ns of each 50 ns umbrella sampling simulation is considered as equilibration and not used in the PMF construction or any other analysis. Calculations of radial pair distribution functions, interaction energies, hydrogen bonds, and number of molecules or atoms within a certain distance of selected part of the system were all performed using the umbrella sampling trajectories with the program VMD.[43] Results of these calculations were further analyzed by binning the data based on ND locations along the z axis and subsequently averaging the data within each 1 Å bin. Standard errors of the results were obtained as $S_i/(N_i/g_i)^{1/2}$, where S_i and N_i are the standard deviation and sample number of bin i, respectively, while g_i is taken as the statistical inefficiency of the umbrella window centered nearest bin i. The calculation of g_i follows Chodera et al.,[55] although instead of truncating the autocorrelation function at 0, we set the threshold to 0.05 to be consistent with that used in g_wham.[54] To characterize the shape of a bilayer, average occupancy of lipid atoms is calculated on a 3D grid with a 1 Å resolution and averaged over all snapshots in a given umbrella window. The occupancy calculation is performed using the VOLMAP[56] plugin of VMD.[43]
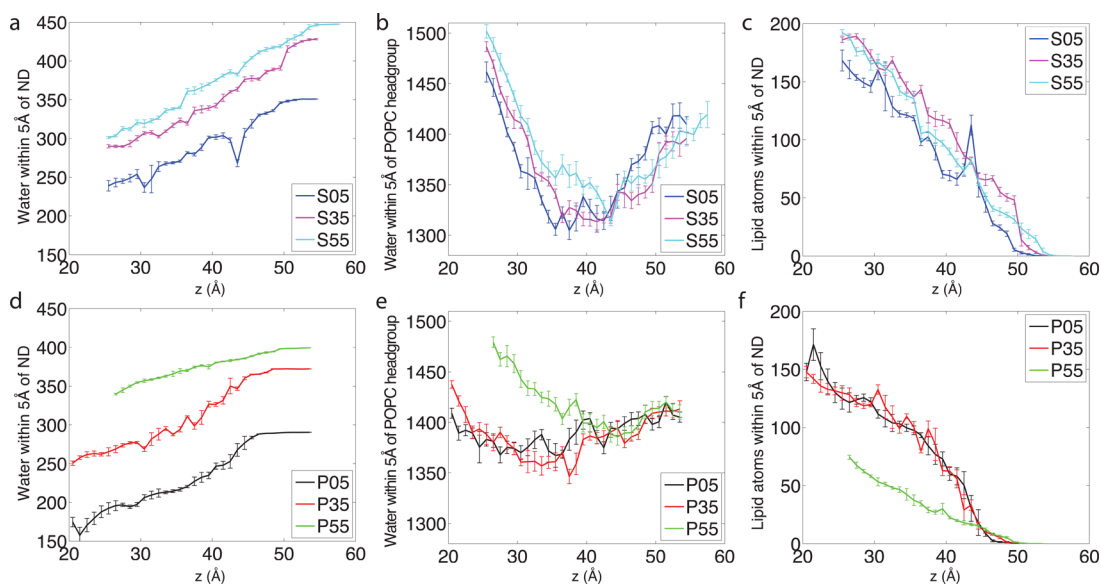
■ RESULTS

We performed a total of 6.5 μs of umbrella sampling calculation to study the energetics and molecular details of nanodimaond−

Figure 3. Snapshots of umbrella sampling simulations of S55. Nitrogen atoms of POPC headgroups are highlighted as blue spheres.
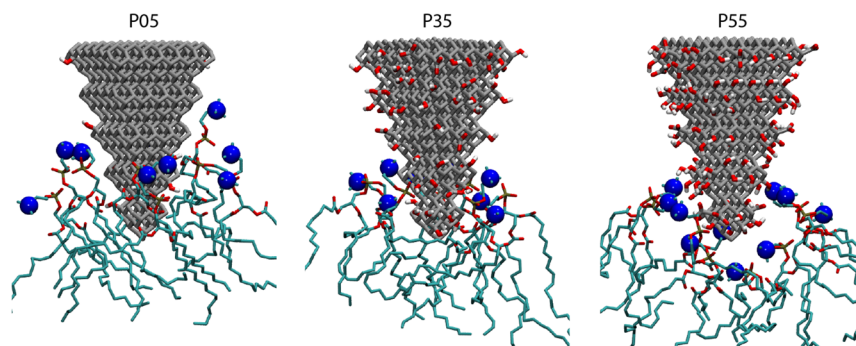

Figure 4. ND−lipid interaction energy changes and the number of ND−lipid hydrogen bonds during umbrella sampling simulations. (a, d) The change in ND−POPC electrostatic interaction energy as the nanodiamonds approach the bilayer. (b, e) The change in ND−POPC vdW interaction energy. (c, f) The total number of ND−POPC hydrogen bonds. All calculations were performed using umbrella sampling trajectories and subsequently binned to yield the average value at a given z (see Methods).

Figure 5. (a, d) Number of water molecules within 5 Å of NDs. (b, e) Number of water molecules within 5 Å of POPC headgroups. (c, f) Number of lipid atoms within 5 Å of NDs. All calculations were performed using umbrella sampling trajectories and subsequently binned to yield the average value at a given z (see Methods).

membrane association. The resulting free energy profiles, as shown in Figure 2, can be divided into two phases, i.e., an

attraction phase and a repulsion phase: as nanodiamonds first approach the membrane, the free energy is generally favorable;

2754

dx.doi.org/10.1021/ct500194s | *J. Chem. Theory Comput.* 2014, 10, 2751−2758

Figure 6. Snapshots of the umbrella sampling simulations of P05, P35, and P55 at the location $z = 27$ Å. Nitrogen atoms of POPC headgroups are highlighted as blue spheres.

this trend is quickly reversed once they become attached to or partially inserted into the membrane. In general, we found that the shape of NDs plays a key role in determining the location of the free energy minima, while their surface functionalization modulates the depth of the minima. Of particular interest are the two modes of ND−membrane interactions revealed by the comparison of spherical and pyramidal NDs: while the former NDs adhere to the bilayer surface, the latter NDs are more likely to anchor in the membrane. Overall, the shape of a nanodiamond largely determines the barrier against its membrane penetration: regardless of surface functionalization, pyramidal NDs have lower barriers of penetrating the bilayer than spherical NDs. Below we discuss these results in detail.

Adhesion of Spherical NDs. Despite small differences, the free energy minima of all three spherical NDs are located within 2 Å of the c.o.m. of upper-monolayer phosphorus atoms ($z \approx 38.4$ Å), indicating their preference for the membrane surface. Figure 3 shows representative snapshots from the umbrella sampling simulation of S55. It is clear that the bilayer is not significantly perturbed when S55 adheres to the membrane. Given its PMF, this result is somewhat expected, as otherwise unfavorable membrane deformation energy will oppose the adhesion of the nanodiamond. However, the absence of membrane deformation alone does not explain the favorable adhesion of NDs to the bilayer. To analyze the driving force of such adhesion, we calculated the interaction energies between the nanodiamond and the POPC lipids. As shown in Figure 4, although the large system size produces significant fluctuation in the data, both electrostatic and vdW interaction energies are found to favor ND-bilayer adhesion. Such favorable interactions with lipids are also reflected in the increased number of hydrogen bonds formed between the nanodiamond and POPC (Figure 4c,f). Qualitatively, adhesion of NDs to the membrane surface also benefits from an entropic gain due to the release of ND-bound as well as lipid-bound water (Figure 5).

The depth of the free energy minima, which measures the strength of ND adhesion, ranges from −9.8 kcal/mol in S05 to −14.7 kcal/mol in S35 and −9.9 kcal/mol in S55. The difference in these values can be partly explained by the different surface hydrophilicity of the NDs: with a largely hydrophobic surface, S05 has the least favorable electrostatic interactions with lipids, although this is somewhat compensated by vdW interactions and a favorable contribution from the release of water (Figure 5). Between S35 and S55, the latter has initially stronger ND−lipid electrostatic interactions, which contribute to a more favorable PMF during the early stage of its adhesion. For example, Figure 3a shows a snapshot of S55 at $z = 54$ Å, where POPC headgroups reach out for the S55 surface. Such behaviors are not observed
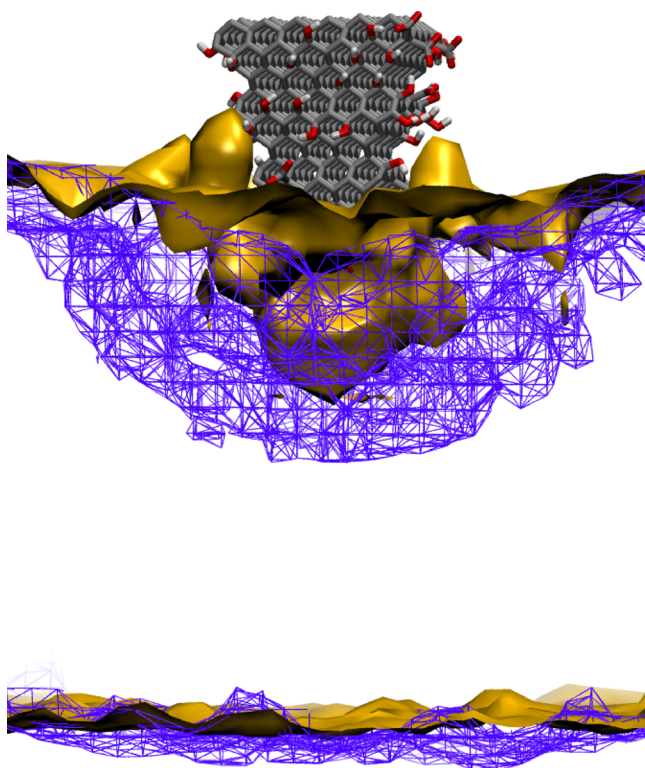
when S05 and S35 are at the same location (data not shown). Nevertheless, as NDs become closer to the bilayer, the highly functionalized surface of S55 and the resulting large solvation shell (Figure 5a) hinders its close contact with the lipids. As shown in Figure 5c, although the number of lipid atoms within 5 Å of the nanodiamond is initially larger in S55, S35 quickly establishes more contact with the bilayer as the two NDs further approach the membrane. The hindered contact of S55 with lipids is also reflected in its smaller number of hydrogen bonds with the bilayer than S35 (Figure 4c). These differences contribute to a weaker free energy minimum in the former ND, which is also slightly shifted away from the bilayer.

Anchoring of Pyramidal NDs. As shown in Figure 4d,e, pyramidal ND−lipid interactions only become significant around $z \approx 48$ Å, reflecting a slower onset than spherical NDs. Furthermore, the free energy minima of P05 and P35 are located below the upper-monolayer phosphorus atoms, suggesting that these NDs prefer to anchor inside the membrane. Specifically, the free energy minima are located at $z = 27$ Å (P05) and $z = 30$ Å (P35), the depth of which is −15.3 kcal/mol and −7.9 kcal/mol, respectively. Unlike these two NDs, P55 has a small free energy minimum (−2.0 kcal/mol) located around $z = 43$ Å. The difference in the above values reflects the different interactions of pyramidal NDs with the lipids: when P05 anchors inside the bilayer, its hydrophobic surface forms favorable contact with lipid tails, which is evident from the snapshot taken at $z = 27$ Å (Figure 6a), where lipid molecules reach out to interact with the P05 surface. Note that these lipids form considerable hydrophobic contact with the P05 surface, which differs from the electrostatic attraction between S55 and lipid headgroups at $z = 54$ Å (Figure 3a). As a result, the most hydrophobic P05 has the strongest attraction to its anchoring position located inside the membrane.

Similar to spherical NDs, water molecules bound to the pyramidal NDs are released when they approach the membrane (Figure 5d). Qualitatively, this provides a favorable entropic contribution to the PMFs, although such contribution appears to be much smaller in P55 than P05 and P35. Similar to S55, the large amount of water surrounding the highly functionalized P55 hinders its bilayer contact, resulting in a smaller number of hydrogen bonds with the lipids than P05 and P35 (Figure 4f). Anchoring of the latter two nanodiamonds may also be facilitated by a favorable contribution from the release of lipid-bound water: the number of water molecules within 5 Å of POPC headgroups is reduced when these two NDs anchor inside the membrane (Figure 5e). This is in clear contrast to P55, where no release of lipid-bound water is observed, and the POPC headgroups are "pushed" deeper to avoid exposing lipid tails to water (Figure 6c). As a consequence, anchoring of P55 is further penalized by

2755

dx.doi.org/10.1021/ct500194s | *J. Chem. Theory Comput.* 2014, 10, 2751−2758

the unfavorable membrane deformation it induces. The location of its free energy minimum ($z = 43$ Å) suggests that P55 prefers to adhere to the membrane. Nevertheless, due to weaker ND−lipid interactions (Figure 4), the depth of P55 free energy minimum is significantly smaller than spherical NDs.

Repulsion due to Membrane Deformation. Once nanodiamonds reach their free energy minima, the PMFs switch to the repulsion phase: an average increase of 42 kcal/mol is observed from the bilayer surface to $z = 25$ Å for spherical NDs. The changes in pyramidal NDs are much smaller: P55 has an increase of ~16 kcal/mol for the same distance, while P05 and P35 have an increase of only 4 and 11 kcal/mol from their anchoring positions, respectively. The amount of free energy increase correlates approximately with the area of membrane deformation induced by the insertion of nanodiamonds: as shown in Figure 7, we calculated the average occupancy of lipid

Figure 7. Membrane deformation caused by P35 and S35. Occupancy of lipid atoms is calculated on a 3D grid with a 1 Å resolution and averaged over all snapshots in the umbrella window centered at $z \approx 26$ Å. Isosurfaces at the value of 0.2 are shown for each ND system (yellow solid surface: P35, purple mesh: S35). For clarity, lipid atoms and S35 are not shown.

atoms in the simulation, which characterizes the average shape of the bilayer. It is clear that the pyramidal ND P35 affects significantly less membrane surface compared with the spherical ND S35. Correspondingly, the free energy increase is much smaller in the former ND. Similar results are observed in the comparison of other NDs with the same surface functionalization (data not shown).

We should note that the size of our simulation systems may have a profound impact on the free energy profiles, especially the repulsion phase. As pointed out by previous studies,[57] a smaller bilayer tends to be more rigid than a larger bilayer during simulations. Such a size effect is particularly evident when particles interact with only one side of the membrane.[58] In our

calculation, this may be found in Figure 7, which shows a highly asymmetric response of the two monolayers to ND-induced membrane deformation. As this effect tends to cancel for simulations performed under the same condition, comparison of NDs with the same shape is less affected than NDs with different shapes. One way to eliminate the size effect is to use the $P2_1$ periodic boundary condition, which approximates a constant chemical potential in the two monlayers.[58] However, such a simulation conditions are not yet widely available. An alternative, which we plan to adopt in our follow-up work, is to simulate bilayers with different sizes and extrapolate the result to a bulk membrane.[57]

■ DISCUSSION

Shape vs Surface Functionalization. The PMFs of the six nanodiamond systems studied here allow us to examine the effect of shape and surface functionalization on ND−membrane association. While detailed free energy profiles clearly depend on both factors, their individual contributions can still be analyzed. Specifically, the effect of shape is primarily found in three aspects: (1) shape plays a key role in determining the location of the free energy minima. With the exception of P55, free energy minima of pyramidal NDs are located inside the membrane, corresponding to an "anchoring" mode, whereas those of spherical NDs are located just above it, corresponding to an "adhesion" mode. The exception of P55 demonstrates that a highly functionalized surface can eliminate the anchoring ability of a nanodiamond. Note, however, that the reverse is not true; i.e., the anchoring ability cannot be gained by simply modifying surface functionalization (all spherical NDs adhere to the membrane). Thus, a proper shape appears to be the prerequisite for NDs to anchor inside the membrane. (2) Shape dictates the strength of attraction before NDs contact the membrane. Figure 2 clearly shows that outside of the membrane, a spherical ND has stronger attraction to the bilayer than its pyramidal counterpart with the same functionalization. As discussed earlier, this likely results from more favorable interactions of the former ND with the lipids, since functional groups on spherical NDs are on average closer to the bilayer. Such difference in spatial distribution of functional groups also produces an earlier onset of the attraction phase in spherical NDs' PMFs. (3) Shape dominates the free energy barrier of the repulsion phase. Once the difference in free energy minima is removed, NDs of the same shape tend to have similar repulsion phases. Although our calculation does not cover the entire bilayer, the trend revealed by the PMFs and membrane deformation indicates that spherical NDs will encounter much higher barriers when they fully penetrate the membrane. These results are in line with recent experimental findings that shape acts as an independent factor in controlling the endosomal escape of nanoparticles.[34]

The effect of surface functionalization is mainly reflected in its modulation of the depth of the free energy minima. The result of such modulation depends on the mode of ND−membrane interactions: for NDs that anchor in the membrane, as they become more functionalized, the depth of their minima decreases, whereas there appears to be an optimal functionalization percentage for NDs that adhere to the membrane. The former result can be explained by the importance of hydrophobic contact in the anchoring of NDs, while the latter reflects the subtlety of ND−membrane adhesion: although very low functionalization is not favored, a highly functionalized surface may in fact weaken the attraction of a ND to the bilayer surface.

Impact of ND Orientation. As described in the Methods section, ND orientation is kept fixed during our simulations (cut surface parallel to the membrane plane). Without calculating a 2D PMF, we may estimate the impact of this missing degree of freedom. Outside of a membrane, spherical NDs experience stronger attraction than pyramidal NDs, which is linked to the functional groups of the former NDs being closer to the membrane. Therefore, once we allow NDs to vary their orientations, the pyramidal ones will likely tilt to maximize favorable ND−membrane interactions, a process that is also favored entropically due to the larger number of states tilted NDs can sample. However, as they further approach the bilayer, the membrane deformation energy associated with large contact area will again favor their initial orientations, which is in line with recent DPD simulation results of nanoparticle translocation across the membrane.[23] We should note that NDs modeled here represent only the tips of nanodiamonds used in a recent experiment,[34] which have an average size of 115 nm and structures more complex than ideal pyramids or spheres. Therefore, a full nanodiamond may adhere to the membrane on a relatively smooth surface, while anchoring its tip on a neighboring surface into the lipid bilayer. During such a process, membrane bending might occur, with the unfavorable bending energy compensated by ND−membrane adhesion strength.

Caveats in Our Calculation. Apart from the size effect discussed earlier, other caveats in our calculation include the limited number of ND models studied here and the approximation used during their construction. Additionally, as only one nanodiamond (spherical or pyramidal) is simulated at a given surface functionalization, the resulting PMFs may be affected by individual differences of the ND models. In another word, two ND models of the same shape and surface functionalization may have different PMFs due to the variance in their spatial distributions of functional groups. Such variance will be more evident in NDs with low surface functionalization. Along this line, the effect of shape on ND surface remains largely unknown experimentally, i.e., whether/how the shape of a ND affects its preferences of various functional groups and/or their distribution. Therefore, apart from enhanced sampling, future modeling work will benefit from more details on the nanodiamond surface as determined by experiments.

CONCLUSIONS

We constructed six atomistic ND models with different shapes or surface functionalization to examine the energetics and molecular details of their membrane association. A total of 6.5 μs umbrella sampling calculation reveals that the nanodiamonds associate favorably with the membrane, which arises from favorable ND−lipid interaction as well as the release of lipid-bound and/or ND-bound water. Comparison of the six ND systems indicates that shape plays a key role in determining the location of the free energy minima, while surface functionalization modulates the depth of the minima. Our calculation provides a quantitative estimate of ND−membrane association strength, which may be used to parametrize future coarse-grained or continuum models, in order to explore nanodiamond−membrane interactions on larger length scales. While we have focused on nanodiamonds in this work, similar all-atom modeling and free energy calculation can be used to characterize the membrane association of other nanoparticles. Such association not only forms the basis of endocytosis but is also the first step in the translocation of these nanoparticles across various cellular membranes.

ASSOCIATED CONTENT

Supporting Information

Figures showing radial pair distribution function of water around ND models and the P05 and S05 nanodiamonds. ND structure files, sample simulation inputs, and force field parameters are also provided. This material is available free of charge via the Internet at http://pubs.acs.org/.

AUTHOR INFORMATION

Corresponding Author
*E-mail: yiwang@phy.cuhk.edu.hk.

Notes
The authors declare no competing financial interest.

REFERENCES

(1) Meng, H.; Liong, M.; Xia, T.; Li, Z.; Ji, Z.; Zink, J. I.; Nel, A. E. *ACS Nano* **2010**, *4*, 4539−4550.
(2) Zhang, X.-Q.; Xu, X.; Bertrand, N.; Pridgen, E.; Swami, A.; Farokhzad, O. C. *Adv. Drug Delivery Rev.* **2012**, *64*, 1363−1384.
(3) Kucsko, G.; Maurer, P.; Yao, N.; Kubo, M.; Noh, H.; Lo, P.; Park, H.; Lukin, M. *Nature* **2013**, *500*, 54−58.
(4) Grant, B. D.; Donaldson, J. G. *Nat. Rev. Mol. Cell Biol.* **2009**, *10*, 597−608.
(5) Huotari, J.; Helenius, A. *EMBO J.* **2011**, *30*, 3481−3500.
(6) Nel, A. E.; Mädler, L.; Velegol, D.; Xia, T.; Hoek, E. M. V.; Somasundaran, P.; Klaessig, F.; Castranova, V.; Thompson, M. *Nat. Mater.* **2009**, *8*, 543−557.
(7) Zhao, F.; Zhao, Y.; Liu, Y.; Chang, X.; Chen, C.; Zhao, Y. *Small* **2011**, *7*, 1322−1337.
(8) Canton, I.; Battaglia, G. *Chem. Soc. Rev.* **2012**, *41*, 2718−2739.
(9) Liu, J.; Sun, Y.; Drubin, D. G.; Oster, G. F. *PLoS Biol.* **2009**, *7*, e1000204.
(10) Zhang, S.; Li, J.; Lykotrafitis, G.; Bao, G.; Suresh, S. *Adv. Mater.* **2009**, *21*, 419−424.
(11) Deserno, M.; Gelbart, W. M. *J. Phys. Chem. B* **2002**, *106*, 5543−5552.
(12) Ruiz-Herrero, T.; Velasco, E.; Hagan, M. F. *J. Phys. Chem. B* **2012**, *116*, 9595−9603.
(13) Gurtovenko, A. A.; Anwar, J.; Vattulainen, I. *Chem. Rev.* **2010**, *110*, 6077−6103.
(14) Wallace, E. J.; Sansom, M. S. P. *Nano Lett.* **2008**, *8*, 2751−2756.
(15) Monticelli, L.; Salonen, E.; Ke, P. C.; Vattulainen, I. *Soft Matter.* **2009**, *5*, 4433−4445.
(16) Shi, X.; von dem Bussche, A.; Hurt, R. H.; Kane, A. B.; Gao, H. *Nat. Nanotechnol.* **2011**, *6*, 714719.
(17) Lin, J.-Q.; Zheng, Y.-G.; Zhang, H.-W.; Chen, Z. *Langmuir* **2011**, *27*, 8323−8332.
(18) Adnan, A.; Lam, R.; Chen, H.; Lee, J.; Schaffer, D. J.; Barnard, A. S.; Schatz, G. C.; Ho, D.; Liu, W. K. *Mol. Pharmaceutics* **2011**, *8*, 368−374.
(19) Marrink, S.; Tieleman, D. *Chem. Soc. Rev.* **2013**, *42*, 6801−6822.
(20) Cooke, I. R.; Deserno, M. *J. Chem. Phys.* **2005**, *123*, 224710.
(21) Vácha, R.; Martinez-Veracoechea, F. J.; Frenkel, D. *Nano Lett.* **2011**, *11*, 5391−5395.
(22) Vácha, R.; Martinez-Veracoechea, F. J.; Frenkel, D. *ACS Nano* **2012**, *6*, 10598−10605.
(23) Yang, K.; Ma, Y.-Q. *Nat. Nanotechnol.* **2010**, *5*, 579583.

(24) Ding, H.-m.; Tian, W.-d.; Ma, Y.-q. *ACS Nano* **2012**, *6*, 1230−1238.

(25) Qiao, R.; Roberts, A. P.; Mount, A. S.; Klaine, S. J.; Ke, P. C. *Nano Lett.* **2007**, *7*, 614−619.

(26) Jusufi, A.; DeVane, R. H.; Shinoda, W.; Klein, M. L. *Soft Mater.* **2011**, *7*, 1139−1146.

(27) Monticelli, L. *J. Chem. Theory Comput.* **2012**, *8*, 1370−1378.

(28) Li, X.; Shi, Y.; Miao, B.; Zhao, Y. *J. Phys. Chem. B* **2012**, *116*, 5391−5397.

(29) Tu, Y.; Lv, M.; Xiu, P.; Huynh, T.; Zhang, M.; Castelli, M.; Liu, Z.; Huang, Q.; Fan, C.; Fang, H.; Zhou, R. *Nat. Nanotechnol.* **2013**, *8*, 594601.

(30) Fang, C.-Y.; Vaijayanthimala, V.; Cheng, C.-A.; Yeh, S.-H.; Chang, C.-F.; Li, C.-L.; Chang, H.-C. *Small* **2011**, *7*, 3363−3370.

(31) McGuinness, L.; Yan, Y.; Stacey, A.; Simpson, D.; Hall, L.; Maclaurin, D.; Prawer, S.; Mulvaney, P.; Wrachtrup, J.; Caruso, F.; Scholten, R.; Hollenberg, L. *Nat. Nanotechnol.* **2011**, *6*, 358−363.

(32) Mochalin, V. N.; Shenderova, O.; Ho, D.; Gogotsi, Y. *Nat. Nanotechnol.* **2012**, *7*, 11−23.

(33) Vanommeslaeghe, K.; Hatcher, E.; Acharya, C.; Kundu, S.; Zhong, S.; Shim, J.; Darian, E.; Guvench, O.; Lopes, P.; Vorobyov, I.; MacKerell, A. D., Jr. *J. Comput. Chem.* **2010**, *31*, 671−690.

(34) Chu, Z.; Zhang, S.; Zhang, B.; Zhang, C.; Fang, C.-Y.; Rehor, I.; Cigler, P.; Chang, H.-C.; Lin, G.; Liu, R.; Li, Q. *Sci. Rep.* **2014**, *4*, 4495.

(35) Chung, P.-H.; Perevedentseva, E.; Tu, J.-S.; Chang, C.; Cheng, C.-L. *Diamond Relat. Mater.* **2006**, *15*, 622−625.

(36) Osswald, S.; Yushin, G.; Mochalin, V.; Kucheyev, S. O.; Gogotsi, Y. *J. Am. Chem. Soc.* **2006**, *128*, 11635−11642.

(37) Iakoubovskii, K.; Mitsuishi, K.; Furuya, K. *Nanotechnology* **2008**, *19*, 155705.

(38) Vanommeslaeghe, K.; MacKerell, A., Jr. *J. Chem. Inf. Model.* **2012**, *52*, 3144−3154.

(39) Vanommeslaeghe, K.; Raman, E. P.; MacKerell, A., Jr. *J. Chem. Inf. Model.* **2012**, *52*, 3155−3168.

(40) Barnard, A. S. *Nanotechnology* **2013**, *24*, 085703.

(41) Hénin, J.; Shinoda, W.; Klein, M. L. *J. Phys. Chem. B* **2008**, *112*, 7008−7015.

(42) Shaw, D. E. et al. *International Symposium on Computer Architecture*; Association for Computing Machinery: New York, 2007; pp 1−12.

(43) Kalé, L.; Skeel, R.; Bhandarkar, M.; Brunner, R.; Gursoy, A.; Krawetz, N.; Phillips, J.; Shinozaki, A.; Varadarajan, K.; Schulten, K. *J. Comput. Phys.* **1999**, *151*, 283−312.

(44) Sotomayor, M.; Schulten, K. *Science* **2007**, *316*, 1144−1148.

(45) Gumbart, J.; Schreiner, E.; Wilson, D. N.; Beckmann, R.; Schulten, K. *Biophys. J.* **2012**, *103*, 331−341.

(46) von Castelmur, E.; Strümpfer, J.; Franke, B.; Bogomolovas, J.; Barbieri, S.; Qadota, H.; Konarev, P. V.; Svergun, D. I.; Labeit, S.; Benian, G. M.; Schulten, K.; Mayans, O. *Proc. Natl. Acad. Sci. U.S.A.* **2012**, *109*, 13608−13613.

(47) Fiorin, G.; Klein, M. L.; Hénin, J. *Mol. Phys.* **2013**, *111*, 3345−3362.

(48) Phillips, J. C.; Braun, R.; Wang, W.; Gumbart, J.; Tajkhorshid, E.; Villa, E.; Chipot, C.; Skeel, R. D.; Kale, L.; Schulten, K. *J. Comput. Chem.* **2005**, *26*, 1781−1802.

(49) Klauda, J. B.; Venable, R. M.; Freites, J. A.; O'Connor, J. W.; Tobias, D. J.; Mondragon-Ramirez, C.; Vorobyov, I.; MacKerell, A. D., Jr.; Pastor, R. W. *J. Phys. Chem. B* **2010**, *114*, 7830−7843.

(50) Andersen, H. C. *J. Chem. Phys.* **1983**, *52*, 24−34.

(51) Miyamoto, S.; Kollman, P. A. *J. Comput. Chem.* **1993**, *13*, 952−962.

(52) Darden, T.; York, D.; Pedersen, L. G. *J. Chem. Phys.* **1993**, *98*, 10089−10092.

(53) Feller, S. E.; Zhang, Y.; Pastor, R. W.; Brooks, B. R. *J. Chem. Phys.* **1995**, *103*, 4613−4621.

(54) Hub, J. S.; de Groot, B. L.; van der Spoel, D. *J. Chem. Theory Comput.* **2010**, *6*, 3713−3720.

(55) Chodera, J. D.; Swope, W. C.; Pitera, J. W.; Seok, C.; Dill, K. A. *J. Chem. Theory Comput.* **2007**, *3*, 26−41.

(56) Cohen, J.; Arkhipov, A.; Braun, R.; Schulten, K. *Biophys. J.* **2006**, *91*, 1844−1857.

(57) Lindahl, E.; Edholm, O. *J. Chem. Phys.* **2000**, *113*, 3882−3893.

(58) Dolan, E. A.; Venable, R. M.; Pastor, R. W.; Brooks, B. R. *Biophys. J.* **2002**, *82*, 2317−2325.